

# The star-formation histories of elliptical galaxies across the fundamental plane

L.A. Nolan<sup>1\*</sup>, J.S. Dunlop<sup>2</sup>, B. Panter<sup>2,3</sup>, Raul Jimenez<sup>4,5</sup>, A. Heavens<sup>2</sup> and G. Smith<sup>2</sup>.

<sup>1</sup>*Astrophysics & Space Science Group, School of Physics and Astronomy, University of Birmingham, Edgbaston, Birmingham, B15 2TT, UK*

<sup>2</sup>*SUPA†, Institute for Astronomy, University of Edinburgh, Royal Observatory, Edinburgh, EH9 3HJ, UK.*

<sup>3</sup>*Max Planck Institute for Astrophysics, Karl-Schwarzschild-Str. 1, Postfach 1317, D-85741 Garching, Germany*

<sup>4</sup>*Department of Physics & Astronomy, University of Pennsylvania, 209 South 33rd Street, Philadelphia, PA 19104-6396, USA*

<sup>5</sup>*The Observatories of the Carnegie Institution, 813 Santa Barbara St., Pasadena, Ca 91101, USA*

Submitted for publication in MNRAS

## ABSTRACT

We present the first results from a study designed to test whether, given high-quality spectrophotometry spanning the mid-ultraviolet–optical wavelength regime, it is possible to distinguish the metal content and star-formation history of individual elliptical galaxies with sufficient accuracy to establish whether their formation history is linked to their detailed morphology and position on the Fundamental Plane.

From a detailed analysis of ultraviolet–optical spectrophotometry of the ‘cuspy’ elliptical galaxy NGC 3605 and the giant elliptical NGC 5018 we find that: 1) optical spectra with  $\lambda > 3500 \text{ \AA}$  may not contain sufficient information to robustly uncover all the stellar populations present in individual galaxies, even in such relatively passive objects as elliptical galaxies, 2) the addition of the ultraviolet data approaching  $\lambda = 2500 \text{ \AA}$  holds the key to establishing well-constrained star-formation histories for these galaxies, from which we can infer a formation and evolution history which is consistent with their photometric properties, 3) despite the superficial similarity of their spectra, the two galaxies have very different ‘recent’ star-formation histories – the smaller, cuspy elliptical NGC 3605 contains a high-metallicity population of age  $\simeq 1 \text{ Gyr}$ , and has a position on the fundamental plane typical of the product of a low-redshift gas-rich merger (most likely at  $z \sim 0.08$ ), while the giant elliptical NGC 5018, with a sub-solar secondary population, appears to have gained its more recent stars via mass transfer / accretion of gas from its spiral companion, 4) despite these differences in detailed history, more than 85% of the stellar mass of both galaxies is associated with an old (9–12 Gyr) stellar population of near-solar metallicity.

This pilot study provides strong motivation for the construction and analysis of high-quality ultraviolet–optical spectra for a substantial sample of ellipticals spanning the fundamental plane.

**Key words:** cosmology: observations – galaxies: evolution – galaxies: formation.

## 1 INTRODUCTION

Despite recent advances in observational cosmology, the formation and evolutionary history of elliptical galaxies remains a controversial subject. Originally thought to be relatively simple, coeval systems (e.g. Faber et al. 1977), the development of hierarchical models in the late 1980s, coupled with the apparent failure of searches for luminous young ellipticals at high redshift, led many workers to the viewpoint that most ellipticals have acquired the bulk of their final mass at relatively low redshift (Kauffmann & Charlot 1998).

In fact, empirical evidence has been presented both for for-

mation of the bulk of the stars in present-day ellipticals at high redshift (Bender et al. 1992; Dunlop et al. 1996; McCarthy et al. 2004; Cimatti et al. 2004; Renzini 2006), and for the formation of ellipticals from the merging of spirals at lower redshift (e.g. Kauffman 1996; Baugh, Cole & Frenk 1996; Baugh et al. 1998; Kauffman & Charlot 1998). A seemingly anti-hierarchical picture has emerged, with the oldest stellar populations residing in the most massive galaxies (De Lucia et al. 2006; Renzini 2006, and references therein).

Recently, however, this long-running debate has taken an interesting turn, with evidence presented that there exist (at least) two distinct classes of elliptical galaxy, which differ in detailed morphology and occupy different areas of the fundamental plane (Kormendy & Bender 1996; Faber et al. 1997). Specifically, some

\* lan@star.sr.bham.ac.uk

† Scottish Universities Physics Alliance

ellipticals have flattened, or ‘core’ central surface brightness distributions, whereas others have power-law, or ‘cuspy’ central surface brightness distributions. The cuspy ellipticals generally have relatively small effective radii, intermediate mass, significant rotational support (Lauer et al. 1995; Faber et al. 1997), and show little or no radio or X-ray emission (Bender et al. 1989). In contrast, the core ellipticals are generally more massive, have large effective radii, are pressure supported with very little rotation (Lauer et al. 1995; Faber et al. 1997), and often show strong radio emission with high X-ray luminosities (Beuing et al. 1999).

Recent N-body merger simulations indicate that equal-mass mergers, or mergers of bulge-dominated systems regardless of the mass ratio, lead to slowly rotating systems with flattened central surface brightness distributions and ‘boxy’ isophotes, while gas-rich unequal-mass mergers produce faster-rotating power-law ellipticals, with ‘disky’ isophotes (Khochfar & Burkert 2005). It has been suggested that the core galaxies had the bulk of their stars in place a long time ago (e.g. Bender et al. 1992), whereas the dissipative mergers producing cuspy ellipticals occurred relatively recently. Genzel et al. (2001) have claimed to find direct evidence of the latter process in action, with their near-infrared study of ULIRGs revealing that these violent gas-rich mergers are heading onto the region of the fundamental plane occupied by power-law ellipticals. This forms an interesting contrast with the discovery by Dunlop et al. (2003) that the hosts of quasars lie in the region of the fundamental plane occupied by giant core ellipticals.

Such an apparently anti-hierarchical picture of elliptical galaxy formation (i.e. in which the most massive objects are the oldest) has received general support from several recent statistical studies (e.g. Kauffman et al. 2003; Caldwell, Rose & Concannon 2003; Heavens et al. 2004), and various theoretical arguments have been advanced to explain how such a situation could arise within a CDM universe in which the growth of the underlying dark matter distribution remains hierarchical. For example, Silk & Rees (1998) argue that outflows driven by the massive and luminous black hole in a young massive galaxy could lead to the ejection of gas and termination of star-formation activity. More recently, Binney (2003) argues that, in the presence of sufficiently dense hot atmosphere, cold infalling gas tends to be ablated and absorbed by the hot atmosphere, preventing any late star-formation activity beyond that produced by the initial infall of cold gas. It has also been argued that the flat cores in the most massive ellipticals may be the result of mergers between two galaxies, each of which already contains a super-massive black-hole (Begelman et al. 1980; Ferrarese & Merritt 2000; Ravindranath, Ho & Filippenko 2002). In this picture, cores could form in the final stages of the merger when the black holes form a binary. Stars are then ejected from the central regions as this binary hardens. Recent N-body simulations support this idea, producing massive core ellipticals from the merging of bulge-dominated galaxies (e.g. Khochfar & Burkert 2005, and references therein).

Despite this wealth of observational and theoretical activity, what is still lacking is a detailed and convincing determination of how elliptical galaxy star-formation histories vary as a function of position on the fundamental plane. If this could be properly established, it would be of enormous assistance in disentangling the relative importance of the different mechanisms for elliptical galaxy formation currently under discussion.

That this has not been achieved despite, for example, the availability of optical spectra for large samples of ellipticals from the Sloan Digital Sky Survey (Eisenstein et al. 2003), may seem surprising but is due to two well known problems. First, there is the

problem of age-metallicity degeneracy, with attempts to determine the ages of stellar populations in elliptical galaxies from optical data being largely foiled by the fact that colours and absorption lines (e.g. Mg) are degenerate to compensating changes in age and metal content (e.g. Worthey 1994; Trager 1999). Second, although progress has been made with the availability of higher-resolution model spectra (e.g. Bruzual & Charlot 2003), there is the problem that with limited spectral range, the data may not allow separation of different stellar age components. For example, while the Balmer lines are only moderately sensitive to changes in metallicity, even small amounts of recent star formation can strengthen the Balmer lines out of all proportion to the actual mass involved in the burst (Trager et al. 2001).

In this paper we present the results of a pilot study designed to test whether, given high-quality expanded wavelength coverage extending into the ultraviolet, these problems can be overcome. Specifically we aimed to test whether, with accurate spectrophotometry spanning  $\lambda \simeq 2500 \rightarrow 8000 \text{ \AA}$ , the age-metallicity degeneracy can be lifted, and the full star-formation history of the elliptical disentangled. Various authors have recognised the potential of near-ultraviolet data to clarify the star-formation history of ellipticals. In particular, Fanelli et al. (1990) found that mid-UV colour and absorption line indices have dependences on temperature and metallicity which are strong and distinct from those derived longward of  $3500 \text{ \AA}$  (Lotz et al. 2000, see also). More recently, Dorman, O’Connell, & Rood (2003) have carried out an extensive exploration of the usefulness of the mid-UV spectral region for determining ages and abundances in old stellar populations, and emphasise the importance of working with low-resolution spectra because of the present inadequacy of high-resolution models.

We sought, therefore, to construct well-calibrated ultraviolet-optical spectra of moderate resolution (i.e.  $5\text{-}10 \text{ \AA}$ ) for elliptical galaxies by combining publically available HST ultraviolet spectroscopy data with existing optical spectrophotometry. NGC 3605 and NGC 5018 transpire to be good representatives of the cuspy and giant core classes of ellipticals respectively.

The structure of the paper is as follows. In the next section we briefly summarise the known properties of NGC 3605 and NGC 5018, and describe the available ultraviolet and optical spectroscopic data which can be combined to produce a properly flux calibrated ultraviolet-optical SED suitable for modelling. Then, in section 3, we describe the model fitting that we have undertaken, exploring models of varying sophistication to determine how complex the star-formation histories of these objects could be, and what results can be regarded as robust. In section 4, we present the results of the model-fitting process, and summarise what can be deduced with confidence from this study about the star formation histories of these two elliptical galaxies. Finally, in Section 5, we consider the implications for elliptical galaxy formation, and discuss the prospects for what could be achieved with a more extensive study, before summarising our conclusions in Section 6.

Throughout this paper we assume a flat cosmology with  $H_0 = 70 \text{ kms}^{-1} \text{ Mpc}^{-1}$ ,  $\Omega_m = 0.3$ , and  $\Omega_\Lambda = 0.7$ . The age of the Universe in this model is 13.5 Gyr.

## 2 DATA

NGC 3605 is an elliptical galaxy with redshift  $z = 0.002228$ , and absolute magnitude  $M_B = -18.48$ . It is a member of the galaxy group NGC 3607. The UV spectrum ( $2260 - 3250$ , and  $3250 - 4760 \text{ \AA}$ ) was observed using the Faint Object Spectrograph

(FOS) on the Hubble Space Telescope (Ponder et al. 1998). The optical spectrum (3520 – 7340 Å) was observed with the FAST spectrograph at the F. L. Whipple Observatory’s 1.5m Tillinghast telescope (Jansen et al. 2000). The FOS observation used a circular 1'' aperture, and the optical spectrum was observed using a 3' x 3'' slit, scanned over a distance equal to half the blue minor-axis optical diameter.

NGC 5018 is a giant elliptical with redshift  $z = 0.009320$  and absolute magnitude  $M_B = -22.22$  (Schweizer & Seitzer 1992). It is a companion to the spiral galaxy NGC 5022. Both an optical (Schweizer & Seitzer 1992) and an HI (Kim et al. 1988) bridge to this galaxy have been observed. The UV spectrum for this galaxy (2260 – 4700 Å) was also observed using FOS on the Hubble Space Telescope (Ponder et al. 1998). The optical spectrum (3709 – 8000 Å) was observed using the Boller and Chivens spectrograph at the ESO 1.52m telescope at La Silla (Bica & Alloin 1987). The final combined spectrum has a total wavelength range 2260 – 8000 Å. Again, the FOS observation used a circular 1'' aperture. The optical spectrum was observed with a 5'' x 8'' slit.

Clearly, the apertures for the UV and optical sections are not matched in either case. We compensate for this in part by allowing the relative normalisation for each spectral segment to float independently where possible (see §3). If there has been a significant episode of star formation in the last few gigayears, one would expect the starburst to have occurred in the central regions, so that the smaller FOS aperture may contain flux from a higher proportion of young stars than the larger optical apertures. However, as the UV region of the SED is likely to be dominated by the flux from young stars anyway (thermally-pulsing asymptotic giant branch stars are not significant contributors to the flux at these wavelengths, (Maraston 2005)), in this case, the leverage for the ratio of young-to-old stars comes mostly from the optical spectrum, which mitigates the effect of un-matched apertures.

The star-formation rate, estimated from [OII]3727 emission, an error on the FOS fluxes of 6%, and the relationship derived by Gallagher, Hunter, & Bushouse (1989) is  $\sim (1\text{-a few}) \times 10^{-4} M_\odot \text{ yr}^{-1}$  for both galaxies, which is as one might expect in early-type galaxies such as these.

The errors on the spectra were estimated for each wavelength bin from the standard deviation of the nearest nine points to that bin, where the bin size was the full width half maximum of the spectral observation (8 Å for the UV spectra, 6 Å for the optical spectrum of NGC 3605, and 11 Å for the optical spectrum of NGC 5018). After the estimation of the errors, the spectra were re-binned, where necessary, to either the resolution of the lowest-resolution section of the stellar population evolutionary synthesis model spectra (10 Å), or, where the resolution of the data was  $> 10$  Å, the models were binned up to match the data (with errors propagated in quadrature).

The resulting spectral energy distributions for these two galaxies are shown in Figure 1.

### 3 MODEL FITTING

We have undertaken our analysis using the most recently updated models of Bruzual & Charlot (2003), hereafter BC03. The age range covered by this model set is 0.01 - 14 Gyr<sup>1</sup>. The models assume that solar metallicity ( $Z_\odot$ ) is 0.02, and the available metallic-

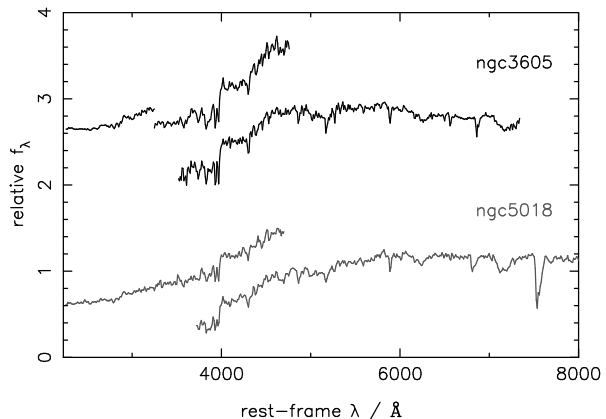


**Figure 1.** The combined UV-optical spectra of the two elliptical galaxies NGC 3605 and NGC 5018. For NGC 3605, the spectra have been rebinned to a resolution of 10 Å. For NGC 5018, the UV portion is at 10 Å resolution, and the optical part at 11 Å. The normalisation is arbitrarily adjusted for clarity.

ities are: 0.02, 0.2, 0.4, 1.0, 2.5  $Z_\odot$ . The wavelength resolution of our data is higher than the outputs generated by the other modelling codes. Although our data could be rebinned to their resolution, our preferred method is to rebin the models and leave the data its least manipulated state.

The galaxy spectra were fitted with synthetic stellar population models in a number of ways. Initially, we have used the MOPED algorithm (Heavens et al. 2000), which allows the initial assumptions about the star formation history to be unconstrained, but does not necessarily return the simplest model consistent with the data. We have then fitted each set of galaxy spectra with a single stellar population, for each available metallicity in turn, with age and relative normalisation allowed to vary freely. Finally, we have fitted a two-component model, in which the age, metallicity and relative mass fraction of the two components are allowed to vary freely. In the latter two cases, the whole parameter space was searched, with the best fit determined via  $\chi^2$  minimisation. The entire available wavelength range longward of 2500 Å for each observed galaxy (i.e. 2500 – 7340 Å for NGC 3605, and 2500 – 8000 Å for NGC 5018) was included in the fits. The sky lines at  $\sim 6600$  Å and  $\sim 7560$  Å were excluded from the fitting in all cases.

#### 3.1 Fitting with the MOPED algorithm

In order to determine the optimal multi-population fit for each spectrum it is necessary to allow as free a star formation history as possible. A parameterization of 11 single stellar populations, spaced logarithmically in time, each with metallicity varying freely, was allowed, together with a one-parameter slab extinction based on the Gordon et al. (2003) LMC curve. We chose to use the LMC extinction curve as it is currently the most reliably characterised dust screen (Gordon et al. 2003). Extensive testing in Panter et al. (2006) has shown that for non star-burst galaxies the choice of extinction curve does not affect the recovered star formation history at optical wavelengths.

In order to fully assess the resulting 23-dimensional likelihood surface it was necessary to use the MOPED<sup>2</sup> (Heavens et al.

<sup>1</sup> The resolution of the age grid of the modelled stellar populations is such that the 14 Gyr population is the closest to the age of the universe. For all

practical purposes the spectrum at this age can be taken to be equivalent to that of a 13.7 Gyr population.

<sup>2</sup> Massively Optimized Parameter Estimation and Data compression

2000; Reichardt et al. 2001) algorithm coupled with a Markov Chain Monte Carlo search method (Panter et al. 2003) developed to deal with the high resolution BC03 models (Panter et al., in preparation). For each galaxy the best solutions from a series of 100 randomly-seeded, conjugate-gradient searches were used to seed a Markov chain of  $10^6$  steps. The individual search traces were examined by eye to confirm full exploration of the parameter space and estimate solution convergence. Due to the speed of the MOPED algorithm this analysis takes of the order three minutes per galaxy on a standard desktop machine, allowing a thorough investigation of a grid of different relative normalisations of the UV, visible and IR spectra, in order to reproduce the star-formation history as accurately as possible.

For both galaxies the individual sections were scaled to optimally match in the overlap region and the final spectra normalised to unity at  $5500\text{\AA}$  then analysed with MOPED (Panter et al. 2006).

### 3.2 Single-metallicity model fits

Each available, single-metallicity, instantaneous starburst model was fitted individually to the spectra of the two galaxies. Each spectral segment (three for NGC 3605, and two for NGC 5018, see Figure 1) was normalised to a mean flux per unit wavelength of unity across its length. For each galaxy, the fit was performed simultaneously on its set of spectra, with the model age varying freely. Unlike the MOPED fits, here we are able to allow the normalisation to vary independently for each section (to compensate for any deviations in the flux calibration). The best-fitting age for each metallicity was found via  $\chi^2$  minimisation.

### 3.3 Two population fits

Finally, a two-population model was constructed, where the age, metallicity and fractional contribution by stellar mass for each component were allowed to vary as free parameters, in order to determine whether more than one significant episode of star formation has occurred. We have

$$F_{2pop,\lambda} = \text{const}(X_i f_{Z_i,\lambda,t_i} + X_j f_{Z_j,\lambda,t_j})$$

Here,  $F_{2pop,\lambda,t}$  is the model flux per unit wavelength in the bin centred on wavelength  $\lambda$  which is the sum of the two single-metallicity model fluxes (per unit wavelength in the bin centred on wavelength  $\lambda$ ),  $f_{Z_i,\lambda,t_i}$  and  $f_{Z_j,\lambda,t_j}$ , which have metallicities and ages,  $Z_i, t_i$  Gyr, and  $Z_j, t_j$  Gyr, respectively. The fractional contributions of the two components,  $X_i$  and  $X_j$ , are allowed to vary freely, and again, normalisation to a mean flux of unity across the wavelength range of each spectral segment was carried out after the addition of the two unnormalised fluxes. As for the single-component model fits, the two-component fitting was carried out simultaneously for each set of galaxy spectra, with the relative normalisation allowed to vary independently.

A minimum- $\chi^2$  fit was used to determine the best-fit values of  $X_i, Z_i, t_i, X_j, Z_j$  and  $t_j$ . Again, the whole parameter space was searched, with the best-fitting parameter values corresponding to the point on the age<sub>*i*</sub>-age<sub>*j*</sub>- $Z_i$ - $Z_j$  grid with the minimum calculated  $\chi^2$ .

## 4 RESULTS

### 4.1 NGC 3605

#### 4.1.1 MOPED result

The spectrum of NGC 3605 was fitted with the MOPED algorithm, and Figure 2 shows the bestfit result of searching the 23-dimensional parameter space with optimal relative normalisation of the UV and optical sections. The results for NGC 3605 are dominated by two populations with central ages of 1.1 and 12 Gyr and metallicity  $Z = 2.32 Z_\odot$  and  $Z = 1.00 Z_\odot$  respectively. The older of the two components accounts for 87% of the total stellar population by mass, and the second component accounts for the remaining 13% of the stellar mass. The dust attenuation associated with the fit is  $E(B - V) = 0.00251$ , consistent with the overall picture of an old elliptical with no recent star formation. The reduced  $\chi^2$  of this fit is 1.774.

#### 4.1.2 Single-metallicity model fit

The results of the single-metallicity fits to the spectra of NGC 3605 are listed in Table 1. For each metallicity, the free parameters are the age and the overall normalisation, which is allowed to vary freely for each section to compensate for any inconsistencies in the flux calibration of the spectral segments. Figure 3 shows the best-fitting single-population model spectrum, superimposed on the observed spectra. The single stellar population model struggles to match the shape of the spectrum in the second segment (3300–4700 Å), and many of the detailed features. This failure is borne out by an unacceptably large value of reduced  $\chi^2$ , namely  $\chi^2_\nu = 2.7$ .

#### 4.1.3 Two population fit

The results for the two-population model fits to the spectrum of NGC 3605 are presented in Table 2 and Figure 4. A young, high-metallicity (1 Gyr,  $2.5 Z_\odot$ ) component is still found, but the fit is much improved by the addition of a dominant mass-fraction of old (10-14 Gyr), lower-metallicity ( $Z_\odot$ ) stars. Degrading the spectral resolution to 20 Å or 40 Å makes no difference to the recovered best-fit parameters, although  $\chi^2_\nu$  decreases to 1.3 and 0.9 respectively.

### 4.2 NGC 5018

#### 4.2.1 MOPED result

The spectrum of NGC 5018 was fitted with the MOPED algorithm, and Figure 5 shows the bestfitting model resulting from searching the 23-dimensional parameter space. The results suggest that NGC 5018 is dominated by a population in the age bin centred on 8.5 Gyr, with metallicity  $Z = 1.50 Z_\odot$  (94% by stellar mass), but has a small contribution (5% by stellar mass) from the age bin centred on 2.3 Gyr, with a metallicity of  $Z = 0.79 Z_\odot$ . There is a very minor (0.07% by stellar mass) population in the bin centred on 1.1 Gyr, with a solar metallicity. The dust attenuation associated with the fit is  $E(B - V) = 0.077$ , consistent with the overall picture of an old elliptical with no recent star formation. The reduced  $\chi^2$  of this fit is 1.39.

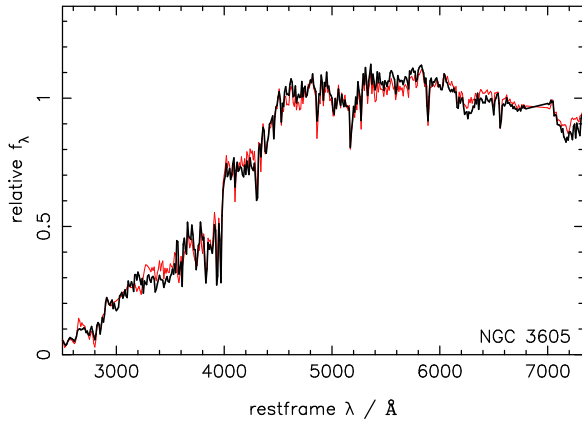


**Figure 2.** Best-fitting model (thin line) to the optimally-spliced spectrum of NGC 3605 (thick line) predicted using MOPED (Heavens et al., 2000). The skylines have been masked out of the fit. The dominant population. has age = 12 Gyr,  $1.00 Z_{\odot}$  and a relative stellar mass fraction of 0.87. There is also a significant (13% by stellar mass) contribution to the flux from a 1.1 Gyr,  $2.32 Z_{\odot}$  population. See section 4.1.1 for discussion.

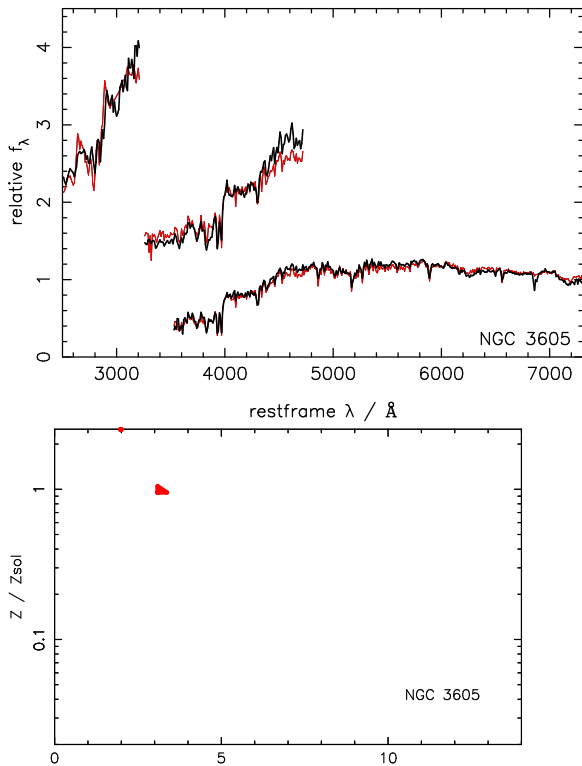


**Figure 3. Top:** the best-fitting single-metallicity model (1 Gyr,  $Z = Z_{\odot}$ , thin black line) superimposed over the spectra of NGC 3605 (thick black line). **Bottom:** the contours enclose the regions where  $\Delta\chi^2 \leq 18.4$ . See section 4.1.2 for discussion.

#### 4.2.2 Single-metallicity model fit

The results of the single-population fits to the spectrum of NGC 5018 are presented in Table 1. Figure 6 shows the observed spectrum, with the best-fit model spectra superimposed. The minimum reduced  $\chi^2$  is  $\chi^2_{\nu} = 3.0$ , from which we may infer NGC 5018 cannot be described by a single, simple stellar population. The best-fit model has an age of 11 Gyr, and solar metallicity. This does not allow the UV flux to be well reproduced.

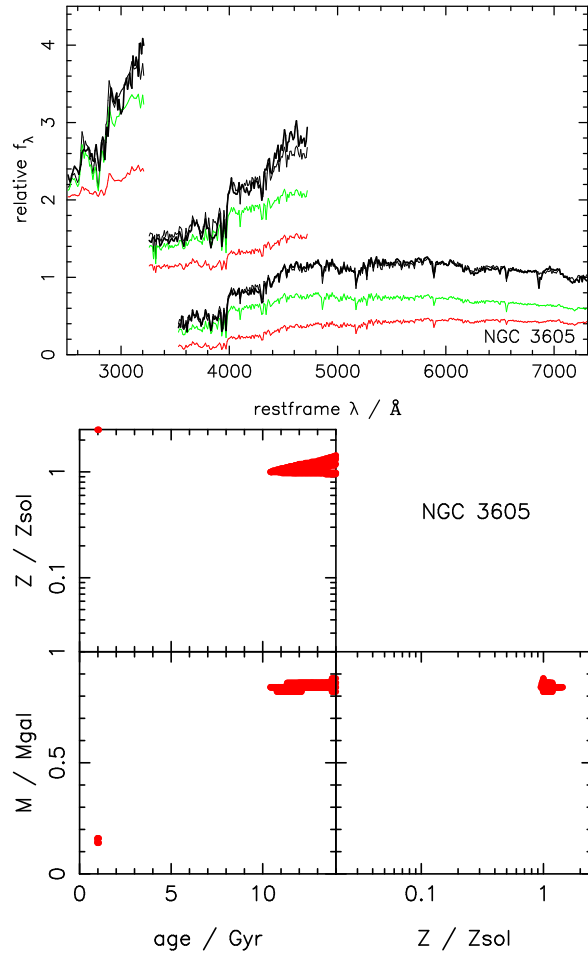


**Figure 4. Top:** the best-fitting two-component model (thin black line) superimposed over the spectral sections of NGC 3605 (thick black line). The two component populations are also shown; the dominant population ( $Z = Z_{\odot}$ , age = 14 Gyr,  $M/M_{gal} = 0.84$ ) is in red, and the secondary stellar population ( $Z = 2.5 Z_{\odot}$ , age = 1 Gyr,  $M/M_{gal} = 0.16$ ) is in green. **Bottom:** the contours enclose the regions where  $\Delta\chi^2 \leq 16.8$ . See section 4.1.3 for discussion.

**Table 1.** Table of results for the single stellar population fits to the spectra of NGC 3605 and NGC 5018. See sections 4.1.2 and 4.2.2 for discussion.

object	$Z / Z_{\odot}$	age / Gyr	min. $\chi^2_{\nu}$
NGC 3605	0.02	14	14.5
	0.2	12	3.5
	0.4	6	3.3
	<b>1.0</b>	<b>3</b>	<b>2.7</b>
	2.5	2	2.7
NGC 5018	0.02	14	52.1
	0.2	14	11.1
	0.4	14	4.2
	<b>1.0</b>	<b>10</b>	<b>3.0</b>
	2.5	3	3.2

**Table 2.** Table of results for the two-component stellar population fits to the spectra of NGC 3605 and NGC 5018. See sections 4.1.3 and 4.2.3 for discussion.

object	$Z / Z_{\odot}$	age / Gyr	$M / M_{gal}$	min. $\chi^2_{\nu}$
NGC 3605	2.5	1	0.16	2.1
	1.0	14	0.84	
NGC 3605 (optical only)	2.5	1	0.12	2.8
	1.0	5	0.88	
NGC 5018	0.4	3	0.12	2.1
	2.5	12	0.88	
NGC 5018 (optical only)	0.02	12	0.14	2.1
	2.5	14	0.86	

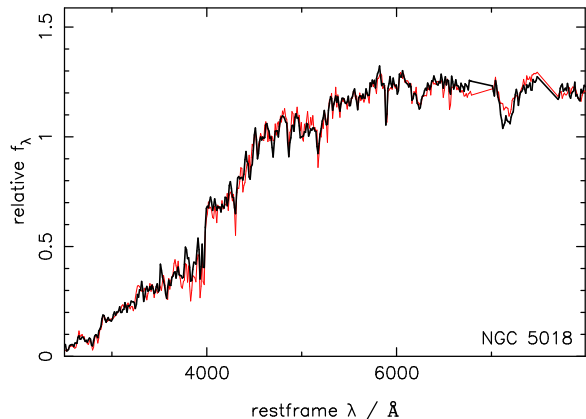


**Figure 5.** The best-fitting model (thin line) to the optimally-spliced spectrum of NGC 5018 (thick line) predicted using MOPED (Heavens et al. 2000). The skylines have been masked out of the fit. The dominant population has age = 8.5 Gyr,  $1.5 Z_{\odot}$  and a relative stellar mass fraction of 0.94. There is also a significant (5% by stellar mass) contribution to the flux from a 2.3 Gyr,  $0.79 Z_{\odot}$  population. See section 4.2.1 for discussion.

#### 4.2.3 Two population fit

The results of the two-population fit to the spectrum of NGC 5018 are presented in Table 2 and Figure 7. The addition of a second, younger component (3 Gyr,  $0.4 Z_{\odot}$ ) significantly improves the fit, particularly shortwards of the 4000 Å break.  $\chi^2_{\nu}$  drops from 3.0 for the single stellar population, to 2.1 with the addition of two extra parameters. Degrading the spectral resolution to 20 Å or 40 Å makes no significant difference to the recovered best-fit parameters.  $\chi^2_{\nu}$  decreases to 1.4 and 1.0 respectively, and at 40 Å resolution the fitting recovers a dominant mature population of 11 Gyr, rather than 12 Gyr.

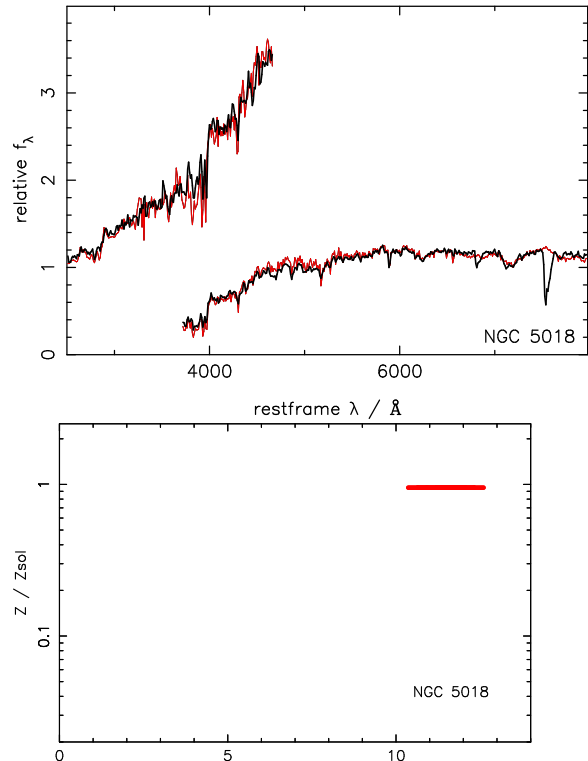


**Figure 6.** **Top:** The best-fitting single-metallicity model (thin black line; age = 11 Gyr,  $Z = Z_{\odot}$ ) super-imposed over the spectral sections of NGC 5018 (thick black line). **Bottom:** the contours enclose the regions where  $\Delta\chi^2 \leq 18.4$ . See section 4.2.2 for discussion.

## 5 DISCUSSION

### 5.1 Age and metallicity determination

In this work, model fits to long-baseline spectra have enabled the age-metallicity degeneracy to be lifted. Comparison of Figures 4 and 8 (for NGC 3605) and of Figures 7 and 9 (for NGC 5018) demonstrates the improvement possible in the simultaneous determination of both age and metallicity when a wide wavelength range is used. In Figures 8 and 9 only the optical (longwards of 3800 Å) spectra have been fitted. Without the leverage from the UV spectra it can be seen that the age of the dominant component in NGC 3605 is almost completely unconstrained, although the young component is still detected. For NGC 5018, although a mature, metal-rich population is recovered, without the extra information provided by the shorter-wavelength data (which are dominated by younger stars) the fitting process instead tries to compensate in matching the shape of the spectrum by choosing a metal-poor mature population. This clearly demonstrates the power of the long-baseline fit in determining age and metallicity, both in constraining the ages and metallicities of the components, and in selecting the correct components.

For NGC 3605, all the detailed fitting (BC03: single stellar population, two-component long-baseline and optical-only fitting) agrees that there is a young (< 3 Gyr), metal-rich component present, but only the long-baseline two-component fitting can constrain the age of the dominant mature population. The results from the full two-component fit are in excellent agreement with the MOPED result.

In Table 3, we compare our one- and two-component fitting using the BC03 models with the best-fitting parameters recovered using models from different authors, namely those of Maraston

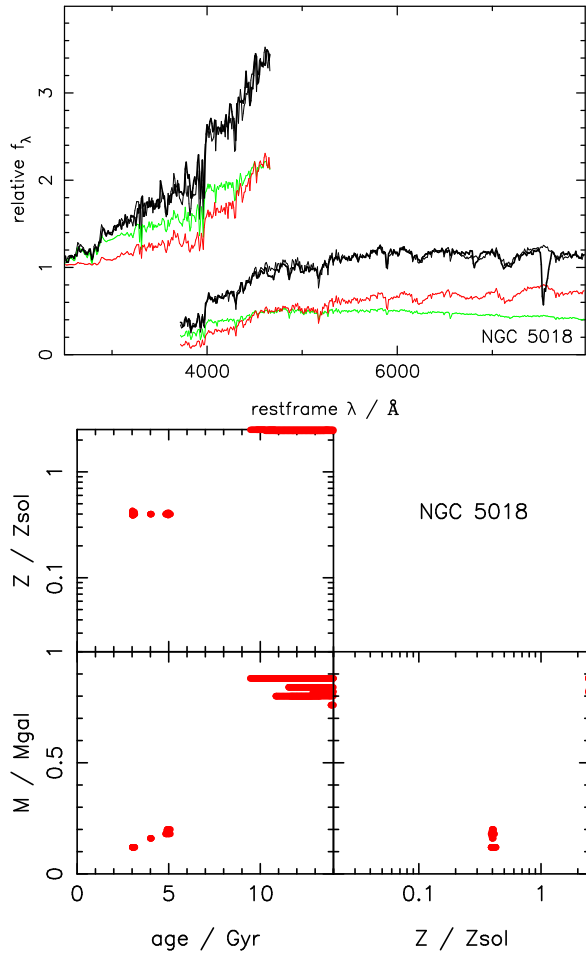


**Figure 7. Top:** the best-fitting two-component model (thin black line) superimposed over the spectral sections of NGC 5018 (thick black line). The two component populations are also shown; the dominant population (age = 12 Gyr,  $Z = 0.4 Z_\odot$ ,  $M/M_{gal} = 0.88$ ) is in red, and the lesser population (age = 3 Gyr,  $Z = 0.4 Z_\odot$ ,  $M/M_{gal} = 0.12$ ) is in green. **Bottom:** the contours enclose the regions where  $\Delta\chi^2 \leq 16.8$ . See section 4.2.3 for discussion.

(2005) and the PEGASE models (Fioc & Rocca-Volmerange 1997). These models have a wavelength resolution of  $20 \text{ \AA}$  (lower than the BC03 models) and, although the age grid is the same for all three model sets, the available metallicities are Maraston (2005): 0.02, 0.5, 1.0, 2.0  $Z_\odot$ , and PEGASE: 0.02, 0.2, 0.4, 1.0, 2.5  $Z_\odot$ . Given the differences between the models, the agreement between the best-fitting parameters recovered for NGC 3605 from the various models is remarkable. The minimum  $\chi^2$  is significantly improved by the addition of a second component, and in all cases, the models find a young ( $\leq 1$  Gyr) secondary component, and a dominant old ( $\geq 12$  Gyr), solar metallicity component. The main difference is that the older PEGASE models do not select the highest available metallicity for the young component, but a solar metallicity instead. However, these results show the robustness of this method to both choice of model and wavelength resolution. The observed 2MASS J-Ks and J-H colours are reproduced by the best-fitting stellar population models to  $\leq \pm 0.15$ . This is a reasonable match, as one might expect some discrepancy between the modelled and observed colours, as the observed colours are those for the entire galaxy, whereas the models represent only those stellar populations residing in the central regions of each galaxy.

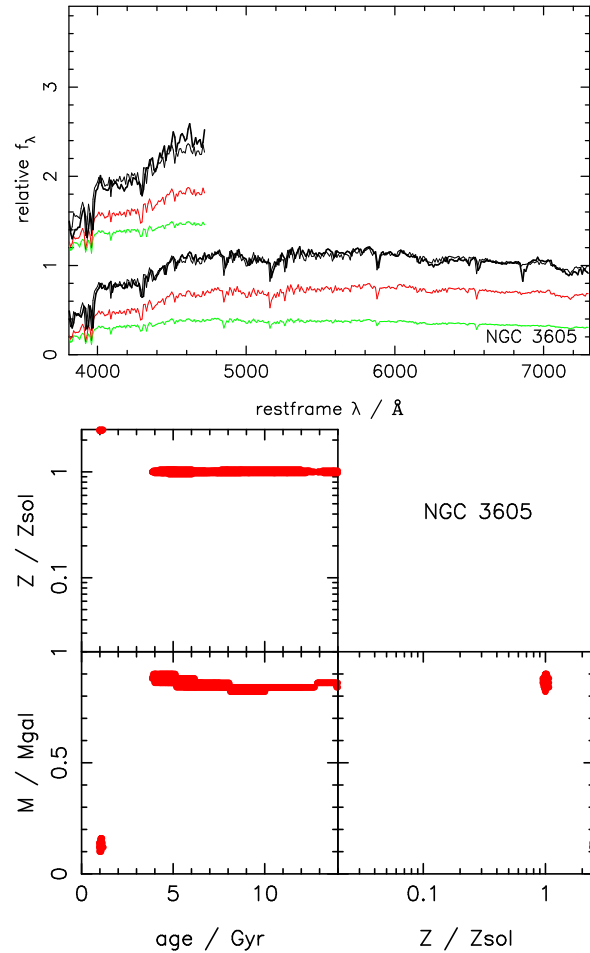


**Figure 8. Top:** the best two-component model (thin black line) fit to the optical-only spectral sections of NGC 3605 (thick black line). The two component populations are also shown; the dominant population (age = 5 Gyr,  $Z = Z_\odot$ ,  $M/M_{gal} = 0.88$ ) is in red, and the lesser population (age = 1 Gyr,  $Z = 2.5 Z_\odot$ ,  $M/M_{gal} = 0.12$ ) is in green. **Bottom:** the contours enclose the regions where  $\Delta\chi^2 \leq 16.8$ . See section 5.1 for discussion.

Terlevich & Forbes (2002) estimated the mean (luminosity-weighted) age of the central region of NGC 3605, by fitting the older stellar population models of Worthey & Ottaviani (1997) to  $H\beta$  and  $[MgFe]$  line indices. They find a mean age of 5.5 Gyr, and a mean metallicity of 1.67  $Z_\odot$ . The high metallicity is consistent with the high metallicity of both our component populations, and the mean age, which may be considered an upper limit to the age of the most recent burst star formation, is also consistent with the presence of the young population that we find.

For NGC 5018, all the detailed BC03 model fits agree that this galaxy is dominated by a mature ( $> 10$  Gyr) metal-rich ( $> Z_\odot$ ) stellar population. The power of the two-component long-baseline fit allows us, in addition, to disentangle the lesser, younger (3–6 Gyr), metal-poor ( $Z = 0.4 Z_\odot$ ) population.

Again, we compare our results from the BC03 models to those recovered from the Maraston and PEGASE models in Table 3. Again, the agreement between the various models is remarkable, demonstrating the robustness of this method. Adding a second component significantly improves the fit, and all the models find a dominant old ( $\geq 12$  Gyr) stellar population, at the highest metallicity available. The BC03 and Maraston models agree that there is a sub-solar metallicity, young (2–3 Gyr) component, although again, the

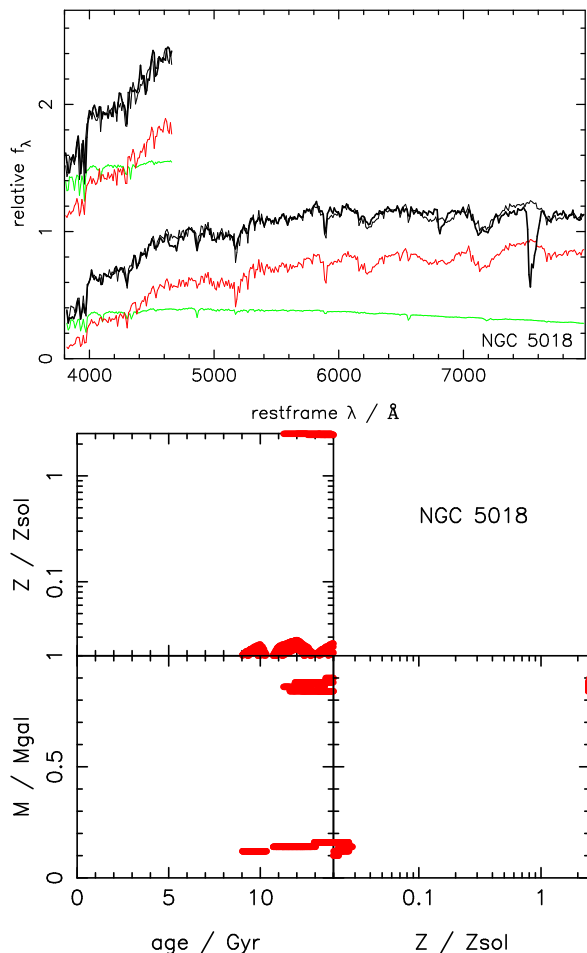


**Figure 9.** **Top:** the best two-component model (thin black line) fit to the optical-only spectral sections of NGC 5018 (thick black line). The two component populations are also shown; the dominant population (age = 14 Gyr,  $Z = 2.5 Z_{\odot}$ ,  $M/M_{gal} = 0.86$ ) is in red, and the lesser population (age = 12 Gyr,  $Z = 0.02 Z_{\odot}$ ,  $M/M_{gal} = 0.14$ ) is in green. **Bottom:** the contours enclose the regions where  $\Delta\chi^2 \leq 16.8$ . See section 5.1 for discussion.

older PEGASE models differ, by selecting an old metal-poor population to fit the blue component. The observed 2MASS colours for NGC 5018 are reasonably well-reproduced by all the models, to  $\leq \pm 0.17$ .

However, using an independent method (comparing the absorption line indices Ca II and  $H\delta/\lambda 4045$ ), and the Worthey (1994) models, Leonardi & Worthey (2000) find that a 2.8 Gyr,  $Z_{\odot}$  population dominates the spectrum of NGC 5018 at 4000 Å. They claim an old, metal-poor population cannot be contributing significantly to the integrated blue light. Our BC03 and Maraston (2005) fitting results are consistent with this. Although our 3 Gyr, 0.4  $Z_{\odot}$  population only accounts for 0.12 % of the stellar mass contributing to the spectrum, it dominates the flux at wavelengths  $\leq 4500$  Å.

More recently, Buson et al. (2004), by matching the HST/FOS UV spectra of NGC 5018 with that of the well-studied compact dwarf elliptical M32, claimed that NGC 5018 is a galaxy whose central regions are dominated by a 3 Gyr stellar population, and that therefore, this galaxy is the child of a major gas-rich merger. They ask the question: ‘is there any evidence of an older stellar population in NGC 5018, or were literally most of the stars we see formed in the merger event?’. Using our long-baseline fitting technique, we can of course answer that question. We do indeed find a

**Table 3.** Comparison of results for the various stellar population model fits to the spectra of NGC 3605 and NGC 5018. See section 5.1 for discussion. The agreement between the different models is excellent.

model	$Z / Z_{\odot}$	age / Gyr	$M / M_{gal}$	min. $\chi^2_D$
<b>NGC 3605</b>				
1-component				
BC03	1.0	3		2.7
Maraston (2005)	2.0	1		1.9
PEGASE (1997)	1.0	3		2.2
2-component				
BC03	1.0	14	0.84	
	2.5	1	0.16	
Maraston (2005)	1.0	14	0.88	1.4
	2.0	0.7	0.12	
PEGASE (1997)	1.0	14	0.94	1.4
	1.0	1	0.06	
<b>NGC 5018</b>				
1-component				
BC03	1.0	10		3.0
Maraston (2005)	0.5	14		3.8
PEGASE (1997)	1.0	10		3.4
2-component				
BC03	2.5	12	0.88	2.1
	0.4	3	0.12	
Maraston (2005)	2.0	14	0.94	2.5
	0.4	2	0.06	
PEGASE (1997)	2.5	11	0.62	2.2
	0.2	14	0.38	

mature stellar population, which dominates the total stellar mass, but, as the young population dominates the flux in the UV, this cannot be detected without using the full spectral range. Conversely, of course, we cannot detect the younger population without including the UV wavelengths.

Although the one- and two-component fitting algorithms do not consider any dust extinction of the spectrum, it is clear from the MOPED results that this is not a large effect in either galaxy. The quality of the fit over an extended baseline endorses the recovered dust parameters, as an error in the dust estimation would result in a gradual offset of the fitting continuum over the length of the spectrum. The one- and two-component fits suffer less in this respect, as the relative normalisations of the sections are allowed to vary.

From the detailed fitting, we do not recover formally acceptable values of  $\chi^2$ . Recent work (e.g. Thomas, Maraston & Bender 2003) has found super-solar  $\alpha$ -element abundances present in early-type galaxies. With non-solar abundances calculated for individual features, they are able to recover better and more consistent fits to absorption-line features than for the solar abundances. Non-solar  $\alpha$ -elements probably account for individual regions of poor fit to the data in this work, but, as long-baseline, non-solar  $\alpha$ -element stellar population models do not as yet exist, we cannot



object	$r_e$ / kpc	$\mu_e$ (K / mag)	$\sigma_0$ / $\text{kms}^{-1}$
NGC 3605	1.9	17.8	103
NGC 5018	4.3	16.6	223
giant core	$7.54 \pm 1.70$	$17.36 \pm 0.68$	$238 \pm 1$
power-law	$2.29 \pm 1.75$	$16.75 \pm 1.00$	$157 \pm 2$

**Table 4.** Observed properties of NGC 3605 and NGC 5018:  $\sigma_0$  is the central velocity dispersion;  $\mu_e$ , the effective surface brightness in the K band, is calculated from the mean surface brightness within the effective half-light radius ( $r_e$ ) in the B band, using  $(B - K) = 3.9$  (Genzel et al., 2001).  $r_e$  for NGC 5018 is from Scorza et al. (1998),  $r_e$  for NGC 3605 is from Faber et al. (1997), and  $\mu_e$  and  $\sigma_0$  for both galaxies is from Faber et al. (1989). Also shown are the mean properties of the galaxy samples plotted in Figure 10. The limits shown are the standard deviation of the sample. All data are taken from Bender et al. (1992), Faber et al. (1997) and Faber et al. (1989).

test whether the quality of the fit will be significantly improved by their use.

Even though, for both galaxies, the vast majority ( $> 99\%$ ) of the stars are reproduced by only two stellar populations, the unrestricted star-formation history permitted by the MOPED algorithm, together with its inclusion of a dust parameter, has enabled a better quality of fit to the two low-redshift elliptical galaxy spectra than that which is possible with even the best-fitting two-population model, i.e. for NGC 3605,  $\chi^2_{\nu} = 1.8$  (compared with 2.1 for the two-component model), and for NGC 5018,  $\chi^2_{\nu} = 1.4$  (also 2.1 for the two-component model).

Despite all of the details discussed above, it is encouraging that, the detailed spectral fits, as well as the MOPED fits, are in good agreement regarding the ages of the populations in these galaxies.

## 5.2 Mergers and the fundamental plane

Figure 10 shows projections in the fundamental plane of the observed properties of NGC 3605 (Faber et al. 1989, 1997) and NGC 5018 (Faber et al. 1989; Scorza et al. 1998), together with a population of giant boxy ellipticals, and intermediate mass, disk ellipticals (Bender et al. 1992; Faber et al. 1997) for comparison. The two galaxy populations occupy different positions in the fundamental plane. Giant ellipticals, with core central surface brightness distributions, tend to be more massive, more luminous and have higher central velocity dispersions than the intermediate-mass ellipticals with power-law central surface brightness distributions ('cuspy' galaxies). Mean values of the effective surface brightness,  $\mu_e$ , effective radius,  $r_e$ , and central velocity dispersion,  $\sigma$ , for the two galaxy populations are listed in Table 4, together with the corresponding values for NGC 3605 and NGC 5018.

The HST/WFPC2 observations of both Faber et al. (1997) and, more recently, Lauer et al. (2005), reveal that NGC 3605 is a cuspy galaxy, and its position on the fundamental plane places it unequivocally in the cuspy galaxy population. The spectroscopic determination of the ages of the constituent populations of NGC 3605 is consistent with the theory that cuspy galaxies are the product of a recent gas-rich galaxy-galaxy merger. The bulk of the stars are old ( $> 10$  Gyr), but there is also a significant young (1 Gyr) stellar population, with a higher metallicity. The higher metallicity is expected to result from the burst of star formation triggered in a recent major gas-rich merger, where the new stars are formed from gas which was metal-enriched when the older stars were formed..

MOPED cannot at present fit multiple spectra simultaneously.

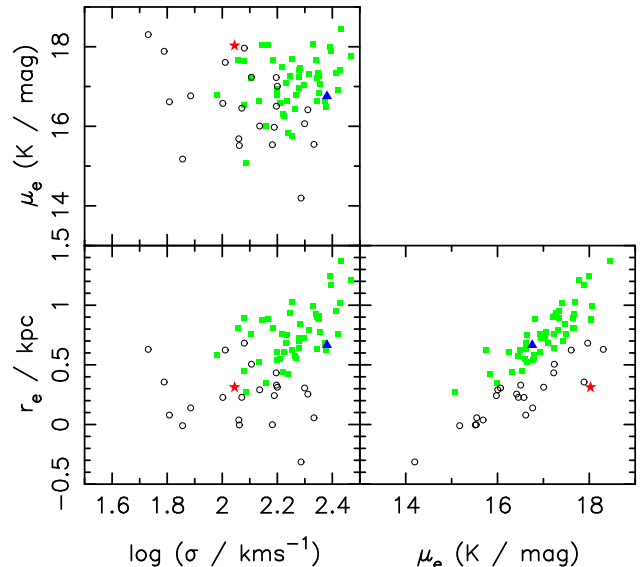


**Figure 10.** Projections of the fundamental plane. Green squares: giant / core ellipticals (from Bender et al., 1992, and Faber et al., 1997); black circles: intermediate mass / power-law ellipticals (from Bender et al., 1992, and Faber et al., 1997); red star: NGC 3605 (from Faber et al., 1989 and Faber et al., 1997); blue triangle: NGC 5018 (from Faber et al., 1989 and Scorza et al., 1998). All parameters are calculated for a cosmology with  $H_0 = 70 \text{ kms}^{-1} \text{ Mpc}^{-1}$  and  $\Omega_m = 0.3$ . See section 5.3 for discussion.

In this case, therefore, adjoining spectral segments were normalised to unity in the overlap regions, and spliced together.

NGC 5018, a shell galaxy, is at first sight more ambiguous. Its effective radius, central velocity dispersion and relatively low  $\mu_e$  suggest that it belongs with the giant core galaxy population, as one might expect from a brightest group elliptical. At the same time, NGC 5018 appears to contain a fairly substantial young population (12% by mass). One might expect this young population to have been triggered by a merger event. However, NGC 5018 is a near companion to the spiral galaxy NGC 5022, and there is evidence of an on-going interaction between these two galaxies: an optical bridge has been detected between them (Schweizer & Seitzer 1992), together with an HI bridge (Kim et al. 1988). Kim et al. conclude that the HI interaction between NGC 5018 and NGC 5022 is current, but Malin & Hadley (1997) infer from the deeply embedded dust lane in NGC 5018 that interactions between the two galaxies have occurred more than once in their history. Simulations indicate that shell structure resulting from a weak interaction between galaxies may survive for a few Gyr (Reduzzi et al. 1996). Therefore, although extra blue light from the shells and bridge mimics a post-merger galaxy, it is more likely that NGC 5018 consists of a predominantly mature central population, which has evolved passively, together with younger shells which are a product of mass transfer or accretion. In addition, the lower metallicity of the younger population ( $0.4 Z_{\odot}$ ) compared with the older population ( $2.5 Z_{\odot}$ ) suggests that the more-recent stars were formed from gas which is either not metal-enriched, or has been diluted by un-enriched gas, which is consistent with star formation triggered by the infall of HI along the bridge between NGC 5018 and NGC 5022. The position of NGC 5018 in the fundamental plane favours this scenario over that of a major merger between two early-type galaxies.

## 6 CONCLUSIONS

We have undertaken a detailed exploration of the star-formation histories of the elliptical galaxies NGC 3605 and NGC 5018. By assembling and analysing the spectral energy distributions of these galaxies spanning the wavelength range 2500 - 8000 Å we aimed to i) determine the added value of the ultraviolet extension for breaking the age-metallicity degeneracy, and disentangling star-formation history, and ii) properly constrain and compare the star-formation histories of these two ellipticals, which occupy very different regions of the fundamental plane. Multi-component stellar population fitting allows us to uncover a far more complete picture of the star-formation history of early-type galaxies than fitting to absorption line features.

We find that i) optical spectra with  $\lambda > 3500$  Å may not contain sufficient information to robustly uncover all the stellar populations present in individual galaxies, even in such relatively passive objects as elliptical galaxies, ii) the addition of the ultraviolet data approaching  $\lambda = 2500$  Å holds the key to uncovering the major epochs of star formation for both galaxies, and establishing well-constrained star-formation histories, from which we can infer a formation and evolution history which is consistent with their photometric properties. Our long-baseline fitting technique is remarkably robust to choice of stellar population model and wavelength resolution iii) despite the superficial similarity of their spectra, the two galaxies have very different star-formation histories – the smaller, cuspy elliptical NGC 3605 contains a high-metallicity population of age 1 Gyr, and has a position on the fundamental plane typical of the product of a low-redshift gas-rich merger, while the giant elliptical NGC 5018, with a sub-solar secondary population, appears to have gained its more recent stars via mass transfer / accretion of gas from its spiral companion, iv) despite these differences in detailed history, more than 85% of the stellar mass of both galaxies is associated with an old (9-12 Gyr) stellar population of near-solar metallicity.

For a universe with  $\Omega_m = 0.3$ ,  $\Omega_\Lambda = 0.7$  and  $H_0 = 70$   $\text{kms}^{-1}\text{Mpc}^{-1}$ , it thus appears that the redshift at which NGC 3605 was assembled to its present state is  $z_{\text{merg}} = 0.076$ , if the formation of the stars in the 1 Gyr population is assumed to have been triggered by this event. This is in agreement with hierarchical structure formation scenarios in which disk-disk merging events take place predominantly at  $z < 1$ . However the vast majority of its stars appear to have formed at  $z_f > 3$ . NGC 5018 also formed the vast majority of its stars at high redshift ( $z_f = 2 - 5$ ), but then appears to have gained a shell (or shells) of younger stars between  $z \simeq 0.3$  and the present-day, possibly through interaction with NGC 5022.

In conclusion, the spectroscopic disentanglement of the component populations of elliptical galaxies is possible, and is a useful tool in the investigation of elliptical galaxy formation and evolution. We are able to determine the formation scenarios of these galaxies, and hence their general position in the fundamental plane using this method. The availability of full SEDs with non-solar  $\alpha$ -element abundances would help to further improve the goodness-of-fit achieved with this method.

## ACKNOWLEDGEMENTS

This work was based in part on observations with the NASA/ESA *Hubble Space Telescope*, obtained at the Space Telescope Science Institute, which is operated by the Association of Universities for Research in Astronomy, Inc. under NASA contract No.

NAS5-26555. Louisa Nolan acknowledges the support of PPARC, through the award of a PDRA. Raul Jimenez is supported by NSF grants AST-0408698 and PIRE-0507768, and NASA grant NNG05GG01G. Ben Panter is supported by the Alexander von Humboldt Foundation, the Federal Ministry of Education and Research, and the Programme for Investment in the Future (ZIP) of the German Government.

## REFERENCES

- Archibald, E. N., Dunlop, J. S., Hughes, D. H., Rawlings, S., Eales, S. A., Ivison, R. J. 2001, MNRAS, 323, 417  
 Baugh C.M., Cole S., Frenk C.S., 1996, MNRAS, 283, 1361  
 Baugh C.M., Cole S., Frenk C.S., Lacey C.G., 1998, ApJ, 498, 504  
 Begelman, M. C., Blandford, R. D., Rees, M. J. 1980, Nature, 287, 307  
 Bender R., Surma P., Dobereiner S., Mollenhoff C., Madejsky R., 1989, A&A, 217, 35  
 Bender R., Burstein D., Faber S.M., 1992, ApJ, 399, 462  
 Beuing J., Dobereiner S., Bohringer H., Bender R., 1999, MNRAS, 302, 209  
 Bica E., Alloin D., 1987, A&A, 186, 49  
 Binney J., 2003, MNRAS, 347, 1093  
 Bruzual, G., Charlot, S. 2003, MNRAS, 344, 1000  
 Buson, L. M., Bertola, F., Bressan, A., Burstein, D., Cappellari, M. 2004, A&A, 423, 965  
 Caldwell N., Rose J.A., Concannon K.D., 2003, ApJ, 125, 2891  
 Cimatti, A., et al. 2004, Nature, 430, 184  
 De Lucia, G., Springel, V., White, S. D. M., Croton, D., & Kauffmann, G. 2006, MNRAS, 366, 499  
 Dorman B., O'Connell R. W., Rood R. T., 2003, ApJ, 591, 878  
 Dunlop J.S., et al., 1996, Nature, 381, 581  
 Dunlop J.S., McLure R.J., Kukula M.J., Baum S., O'Dea C.P., Hughes D.H., 2003, MNRAS, 340, 1095  
 Eisenstein D.J., et al., 2003, ApJ, 585, 694  
 Faber S.M., et al., 1997, AJ, 114, 1771  
 Faber, S. M., Wegner, G., Burstein, D., Davies, R. L., Dressler, A., Lynden-Bell, D., Terlevich, R. J. 1989, APJS, 69, 763  
 Faber S.M., et al., 1997, AJ, 114, 1771  
 Fanelli M.N., O'Connell R.W., Burstein D., Wu C.-C., 1990, ApJ, 364, 272  
 Ferrarese, L., Merritt, D. 2000, ApJL, 539, L9  
 Fioc M., Rocca-Volmerange B., 1997, A&A, 326, 950  
 Gallagher J. S., Hunter D. A., Bushouse H., 1989, AJ, 97, 700  
 Genzel R., et al., 2001, ApJ, 563, 527  
 Gordon K. D., Clayton G. C., Misselt K. A., Landolt A. U., Wolff M. J., 2003, ApJ, 594, 279  
 Heavens, A.F., Panter, B.D., Jimenez, R., Dunlop, J.S., 2004, Nature, 428, 625  
 Jansen, R. A., Fabricant, D., Franx, M., Caldwell, N. 2000, ApJS, 126, 331  
 Heavens, A. F., Jimenez, R., Lahav, O. 2000, MNRAS, 317, 965  
 Kauffman G., 1996, MNRAS, 281, 487  
 Kauffmann, G., & Charlot, S. 1998, MNRAS, 294, 705  
 Kauffman G., Charlot, S. 1998, MNRAS, 297, L23  
 Kauffman G., et al., 2003, MNRAS, 341, 54  
 Khochfar, S., & Burkert, A. 2005, MNRAS, 359, 1379  
 Kim, D.-W., Jura, M., Guhathakurta, P., Knapp, G. R., & van Gorkom, J. H. 1988, ApJ, 330, 684  
 Kormendy J., Bender R., 1996, ApJL, 464, L119

- Lauer T.R., et al., 1995, AJ, 110, 2622  
Lauer, T. R., et al. 2005, AJ, 129, 2138  
Khochfar, S., & Burkert, A. 2005, MNRAS, 359, 1379  
Lotz J.M., Ferguson H.C., Bohlin R.C., 2000, ApJ, 532, 830  
Malin, D., & Hadley, B. 1997, Publications of the Astronomical Society of Australia, 14, 52  
Maraston, C., 2005, MNRAS, 362, 799  
McCarthy, P. J., et al. 2004, ApJL, 614, L9  
Panter, B., Heavens, A. F., & Jimenez, R. 2003, MNRAS, 343, 1145  
Panter, B., Jimenez, R., Heavens, A. F & Charlot, S., 2006, submitted to MNRAS, astro-ph/0608531  
Ponder, J. M., et al. 1998, AJ, 116, 2297  
Ravindranath S., Ho L.C., Filippenko A.V., 2002, ApJ, 566, 801  
Reduzzi, L., Longhetti, M., & Rampazzo, R. 1996, MNRAS, 282, 149  
Reichardt, C., Jimenez, R., Heavens, A. F. 2001, MNRAS, 327, 849  
Renzini, A., 2006 astro-ph/0603479, to appear on Annual Review of Astronomy & Astrophysics, Vol. 44  
Scorza, C., Bender, R., Winkelmann, C., Capaccioli, M., & Macchetto, D. F. 1998, A&AS, 131, 265  
Scott, S. E., et al. 2002, MNRAS, 331, 817  
Schweizer, F., Seitzer, P. 1992, AJ, 104, 1039  
Silk, J., Rees, M. J. 1998, A&A, 331, L1  
Stevens, J. A., et al. 2003, Nature, 425, 264  
Terlevich, A. I., Forbes, D. A. 2002, MNRAS, 330, 547  
Thomas, D., Maraston, C., Bender, R. 2003, MNRAS, 339, 897  
Trager S.C., 1999, In: Photometric Redshifts & High-z galaxies, ASP Conf Ser vol 191, p.195  
Trager S.C., et al., 2001, In: Astrophysical Ages and Time Scales, (astro-ph/0104404)  
Worthey G., 1994, ApJS, 95, 107  
Worthey, G., Ottaviani, D. L. 1997, ApJS, 111, 377